NONLINEAR POLARISATION EFFECTS IN FIBRE-BASED EXTREME LEARNING MACHINES

Lilian EMONIN[1], Andrei V. ERMOLAEV[1], Mathilde HARY[1], Anas SKALLI[1], Daniel BRUNNER[1], Christophe FINOT[2], Goëry GENTY[3], John M. DUDLEY[1]

[1] *Université Marie et Louis Pasteur, CNRS Institut FEMTO-ST, 25000 Besançon, France*
[2] *Université Bourgogne Europe, CNRS Laboratoire Interdisciplinaire Carnot de Bourgogne, 21078 Dijon, France*
[3] *Photonics Laboratory, Tampere University, FI-33104 Tampere, Finland*

lilian.emonin@femto-st.fr

RÉSUMÉ

Optical fibre-based extreme learning machines (ELMs) are a powerful physical platform for unconventional computing. However, although experiments have reported promising results exploiting supercontinuum and wave-breaking dynamics, there has been much less work developing theoretical or numerical models to determine the computational limits of such systems. Here, we use coupled vectorial generalized nonlinear Schrödinger equations to present the first numerical study of fibre ELMs taking into account polarisation effects during propagation. Our results establish a foundation for designing and interpreting polarisation sensitive nonlinear fibre-based ELM platforms

MOTS-CLEFS : *photonic machine learning ; vectorial nonlinear fibre optics.*

Fibre-based extreme learning machines (ELMs) perform task-specific computation by exploiting nonlinear propagation dynamics in optical fibre [1]. There has been intense recent experimental activity in this field by multiple groups [2–5], demonstrating ELMs based on both anomalous-dispersion regime supercontinuum generation [6, 7] and normal-dispersion wave-breaking dynamics [8]. Building on this progress, numerical studies of fibre ELM systems have also been reported, using the scalar generalized nonlinear Schrödinger equation (GNLSE) to examine how performance depends on the physical system parameters [9, 10].

Here, we extend this numerical framework to present the first study of fibre-based ELM performance including full vectorial (polarisation) effects. Our modelling uses coupled vectorial GNLSEs incorporating birefringence, Raman scattering, self-steepening, and higher-order dispersion [8, 11]. We explore how ELM classification accuracy for the MNIST handwritten digits dataset depends both on the input polarisation state as well as different approaches to polarisation-dependent readout, and we present results for both anomalous- and normal-dispersion regime propagation. Our results show that polarisation effects can introduce a detrimental effect into the ELM classification accuracy unless care is taken to suitably analyse the output ELM polarization state.

Our simulations solve the well-known coupled GNLSEs previously used to model vectorial supercontinuum generation [8, 11, 12]. For circular polarisation components u_1 and u_2, we have :

$$\begin{aligned}\frac{\partial u_j}{\partial z} = &\left(i\frac{\Delta\beta_0}{2} - \frac{\Delta\beta_1}{2}\frac{\partial}{\partial\tau}\right)u_{3-j} - i\left(\frac{\beta_2}{2!}\frac{\partial^2}{\partial\tau^2} + i\frac{\beta_3}{3!}\frac{\partial^3}{\partial\tau^3} + \cdots\right)u_j \\ &+ i\gamma\left(1 + \frac{i}{\omega_0}\frac{\partial}{\partial\tau}\right)\left\{(1-f_R)\left(\frac{2}{3}|u_j|^2 + \frac{4}{3}|u_{3-j}|^2\right)u_j\right. \\ &\left. + f_R\, u_j \int_{-\infty}^{\tau} h_R(\tau-\tau')\left[|u_j(\tau')|^2 + |u_{3-j}(\tau')|^2\right]d\tau'\right\}\end{aligned} \tag{1}$$

Here indices $j = 1, 2$, z is distance, τ is time, the β_k are the k^{th}-order dispersion coefficients at ω_0, γ is the nonlinear coefficient, h_R is Raman response of silica [11] with $f_R = 0.18$. The linear field

components along principal axes x and y are $E_x = [(u_1 + u_2)/\sqrt{2}]\exp(-i\Delta\beta_0 z/2)$, and $E_y = [(u_1 - u_2)/i\sqrt{2}]\exp(i\Delta\beta_0 z/2)$. The birefringence-induced phase and group mismatches are $\Delta\beta_0$ and $\Delta\beta_1$ respectively, with $\Delta\beta_0 = \omega_0\Delta n/c$ and $\Delta\beta_1 = v_x^{-1} - v_y^{-1}$. Here $\Delta n = n_x - n_y$ is the refractive-index difference and v_x and v_y are the group velocities along the two axes. We consider a pump wavelength of 1550 nm and fibre properties as in Ref. [9]. For anomalous-dispersion regime propagation in 70 m fibre, we take : $\beta_2 = -0.12\,\mathrm{ps^2km^{-1}}$; $\beta_3 = 0.040\,\mathrm{ps^3km^{-1}}$; $\beta_4 = 0\,\mathrm{ps^4km^{-1}}$; $\gamma = 10.7\ \mathrm{W^{-1}km^{-1}}$; for normal-dispersion regime propagation in 40 m of fibre, we take : $\beta_2 = 0.987\,\mathrm{ps^2km^{-1}}$; $\beta_3 = 7.31\times10^{-3}\,\mathrm{ps^3km^{-1}}$; $\beta_4 = 4.10\times10^{-4}\,\mathrm{ps^4km^{-1}}$; $\gamma = 7.5\ \mathrm{W^{-1}km^{-1}}$. We used linearly-polarised input pulses with Jones matrices applied to vary the input polarisation relative to the fibre principal axes, as well as to analyse the polarisation properties of the output along specific directions.

Fig. 1 shows typical results. We consider propagation in birefringent fibre with $\Delta n = 10^{-5}$. Input pulses have ∼150 fs duration and ∼10 nm bandwidth, with ∼100 W or ∼1200 W peak power for anomalous or normal dispersion regime propagation respectively. A length-100 compressed representation of an MNIST handwritten digit image is scaled to maximum value of 0.25π and used to spectrally phase-encode a pulse prior to fibre injection. Nonlinear and dispersive propagation in the fibre then leads to spectral broadening over 200 nm and dimensional expansion of the encoded information. A standard ELM approach is used, repeating this procedure for 60000 MNIST images to yield an effective hidden-layer matrix of 60000 broadened spectra. The known digit labels allow us to compute the output layer weight matrix via regression (Penrose-Moore or ridge) in one step i.e. avoiding iterative training using backpropagation. Performance is evaluated by applying the weight matrix to a validation set of 10000 spectra generated from input pulses encoded using previously unseen images, and comparing the predicted labels with the known inputs to evaluate quantitative percentage accuracy for digit classification.

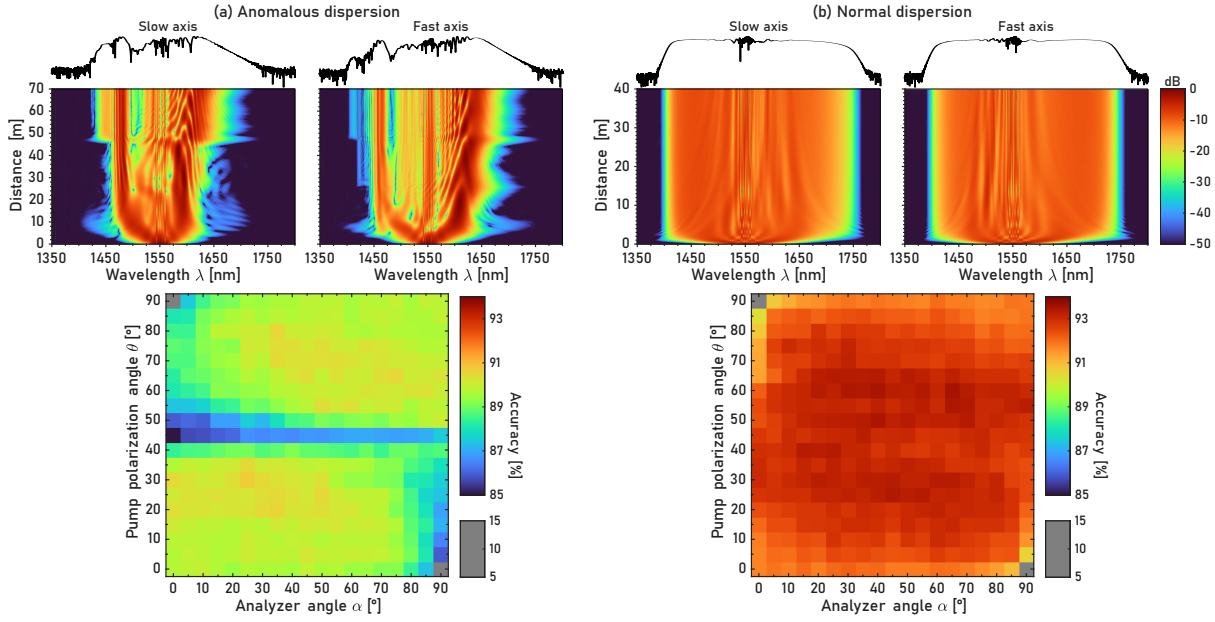


FIGURE 1 : (a) and (b) show results for anomalous and normal dispersion respectively. The upper plots show spectral evolution on slow and fast axes as indicated. The heatmap shows the MNIST classification accuracy (colourbar on the right) varying the linear polarisation angle of the injected input (vertical axis) and for different polarisation selection readout angles for the output spectra (horizontal axis).

To study how nonlinear polarisation dynamics impact ELM performance, we varied the injection angle θ of the linearly-polarised input pulses relative to the principal axes, and analysed the output spectrum along specific polarisation directions set by an analysing angle α. For anomalous and normal dispersion regime propagation respectively, Figs 1(a) and (b) first show the spectral evolution along the

two fibre axes for a particular input pulse injected at 45°. These results show how spectral structure along each axis can be very different in both overall width and/or fine structure and indeed, how the spectral broadening develops for each particular input angle depends sensitively on the fibre and pulse parameters [11]. To study the impact of this on ELM accuracy, we performed the training and test procedure described above for input injection angles from $0-90°$ (measured relative to the slow axis) and we also created different hidden layer matrices by analysing the output spectra in each case along different projected directions over $0-90°$. The heatmaps in Fig. 1 show how the ELM accuracy (see colourbar) depends on both the input and readout polarisation direction, with greater variation for anomalous dispersion. Indeed, for anomalous dispersion, the accuracy can even fall below the pure linear regression benchmark of $\sim$85% for certain pump-readout combinations, although it can reach up to 91% with careful optimisation. As also observed in the scalar case [9], performance is better for normal dispersion up to 93%, and our modelling here also reveals the important result that normal dispersion spectral broadening it is much less sensitive to polarisation.

Overall, these results provide important additional design guidelines for fibre-based ELM, further supporting the superior performance seen with propagation dynamics driven by normal dispersion wave-breaking over anomalous dispersion supercontinuum. We will also present results of further simulations studying the effect of random birefringence, and polarisation-independent readout.

RÉFÉRENCES

[1] G. Marcucci, D. Pierangeli, and C. Conti, "Theory of neuromorphic computing by waves : Machine learning by rogue waves, dispersive shocks, and solitons," *Physical Review Letters*, vol. 125, p. 093901, 2020.

[2] B. Fischer, M. Chemnitz, Y. Zhu, N. Perron, P. Roztocki, B. Maclellan, L. Di Lauro, A. Aadhi, C. Rimoldi, T. H. Falk, and R. Morandotti, "Neuromorphic computing via fission-based broadband frequency generation," *Advanced Science*, vol. 10, p. 2303835, 2023.

[3] K. F. Lee and M. E. Fermann, "Supercontinuum neural network and analog computing evaluation," *Physical Review A*, vol. 109, no. 3, p. 033521, 2024.

[4] S. Saeed, M. Müftüoglu, G. R. Cheeran, T. Bocklitz, B. Fischer, and M. Chemnitz, "Nonlinear inference capacity of fiber-optical extreme learning machines," *Nanophotonics*, vol. 14, pp. 2749–2760, 2025.

[5] M. Hary, D. Brunner, L. Leybov, P. Ryczkowski, J. M. Dudley, and G. Genty, "Principles and metrics of extreme learning machines using a highly nonlinear fiber," *Nanophotonics*, vol. 14, pp. 2733–2748, 2025.

[6] J. M. Dudley, G. Genty, and S. Coen, "Supercontinuum generation in photonic crystal fiber," *Reviews of Modern Physics*, vol. 78, pp. 1135–1184, 2006.

[7] J. M. Dudley, G. Genty, A. Heidt, T. Sylvestre, J. C. Travers, and J. R. Taylor, "Fibre supercontinuum generation : Progress and perspectives," *Europhysics Letters EPL*, vol. 151, no. 5, p. 55001, 2025.

[8] G. P. Agrawal, *Nonlinear Fiber Optics*. Elsevier, 2019.

[9] A. V. Ermolaev, M. Hary, L. Leybov, P. Ryczkowski, A. Skalli, D. Brunner, G. Genty, and J. M. Dudley, "Limits of nonlinear and dispersive fiber propagation for an optical fiber-based extreme learning machine," *Optics Letters*, vol. 50, no. 13, p. 4166, 2025.

[10] I. Muda, A. Maula, and U. Teğin, "Optical computing with supercontinuum generation in photonic crystal fibers," *Optics Express*, vol. 33, no. 4, pp. 7852–7861, 2025.

[11] Z. Zhu and T. G. Brown, "Polarization properties of supercontinuum spectra generated in birefringent photonic crystal fibers," *Journal of the Optical Society of America B*, vol. 21, pp. 249–257, 2004.

[12] S. Coen, A. H. L. Chau, R. Leonhardt, J. D. Harvey, J. C. Knight, W. J. Wadsworth, and P. S. J. Russell, "Supercontinuum generation by stimulated raman scattering and parametric four-wave mixing in photonic crystal fibers," *Journal of the Optical Society of America B*, vol. 19, pp. 753–764, 2002.